

Theory of excitonic order in kagome metal ScV_6Sn_6

Julian Ingham,^{1,*} Armando Consiglio,² Domenico di Sante,³ Ronny Thomale,^{4,5,†} and Harley D. Scammell⁶

¹*Department of Physics, Columbia University, New York, NY, 10027, USA*

²*Istituto Officina dei Materiali, Consiglio Nazionale delle Ricerche, Trieste I-34149, Italy*

³*Department of Physics and Astronomy, University of Bologna, 40127 Bologna, Italy*

⁴*Institute for Theoretical Physics and Astrophysics,
University of Würzburg, D-97074 Würzburg, Germany*

⁵*Department of Physics and Quantum Centers in Diamond and Emerging Materials (QuCenDiEM) Group,
Indian Institute of Technology Madras, Chennai, India*

⁶*School of Mathematical and Physical Sciences, University of Technology Sydney, Ultimo, NSW 2007, Australia*

(Dated: October 28, 2024)

We argue that kagome metals can feature an excitonic condensate of unconventional nature. Studying the recently discovered variant ScV_6Sn_6 , we identify electron and hole pockets due to a pair of van Hove singularities (vHS) close to the Fermi level, with an approximate spectral particle-hole symmetry at low energies. A significant fraction of the Fermi level density of states away from the vHS is removed by the onset of high temperature charge density wave order, and makes the bands more two dimensional, setting the stage for the formation of excitons. We develop a two-orbital minimal model which captures these features, along with the sublattice support of the wavefunctions, and find s -wave or d -wave excitons depending on the microscopic interaction parameters – the latter of which exhibits either a charge nematic or time-reversal symmetry breaking flux order depending on strain, offering an explanation of recent STM and transport experiments. The appearance of particle-type and hole-type vHS, and the excitonic resonance associated with it, may be a common thread to understanding nematicity and time-reversal symmetry breaking in kagome metals.

Introduction. The kagome pattern – consisting of a network of corner sharing triangles – has long been seen as a promising motif in the search for materials hosting novel physics [1–6]. In the last decade, increasing attention has been directed towards kagome metals, offering a rich kinematic phenomenology involving Dirac points, flat bands and van Hove singularities (vHS) as a function of Fermi level [7, 8]. As compared to previous studies of correlated electrons in hexagonal systems such as the triangular lattice or the honeycomb lattice, the kagome lattice stands out in that vHS are naturally prone to appear in the vicinity of the Fermi level.

As a common thread to electronic orders discovered thus far in kagome metals, such as the V-based AV_3Sb_5 ($A=\text{K},\text{Rb},\text{Cs}$) [9–11], or Ti-based ATi_3Bi_5 [12, 13], a high-temperature charge order appears, followed by a superconducting transition at lower temperature. Compound-dependant differentiations proliferate with regard to the precise nature of charge order and superconductivity – ranging from rotational and time-reversal symmetry breaking, as well as the possibility of pair density wave or a unit-cell modulated superconducting pairing [14–20].

Excitons are emergent bound states formed in insulators and semiconductors between a electron-like and hole-like carrier, where the binding energy derives from Coulomb interactions. The constraints on the band structure of a crystal in which such excitons may form, and be experimentally resolvable, are manifold. An idealized toy model comprises a valence and conduction band of oppo-

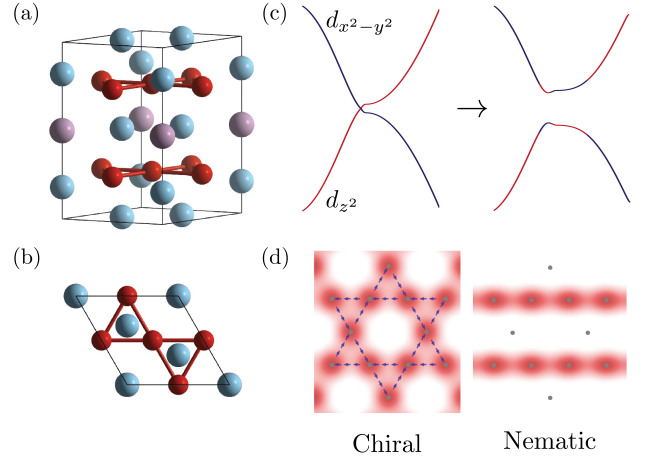


FIG. 1: **Excitonic orbital order in 166 kagome metal ScV_6Sn_6 .** The crystal structure of ScV_6Sn_6 : (a) standard and (b) top-view of the pristine unit cell ($\text{V} = \text{red}$, $\text{Sc} = \text{violet}$, $\text{Sn} = \text{blue}$). (c) The presence of oppositely dispersing vHS results in a weak coupling instability towards an excitonic state which hybridizes the two bands, producing either flux (d, left) or nematic order (d, right).

site curvature, and neglects exciton decay via additional bands or other midgap states. As with any other two-particle state, the excitonic particle-hole pair relates to an irreducible point group representation (irrep) and inherits its specific form from the spin and orbital nature of the underlying electronic degrees of freedom. If the gap is small, or even zero in the case of a semimetal, the exciton energy can become negative, triggering Bose condensation and a symmetry-breaking ground state [21–23].

In this Letter, we develop a theory of excitonic resonances in kagome metals. Exploiting the abundance of

*ji2322@columbia.edu

†ronny.thomale@uni-wuerzburg.de

vHS around pristine filling in kagome metals, we consider the case where opposite concavity vHS occur at a similar distance from the Fermi level. A properly chosen charge order can effectively convert a kagome metal to a ‘kagome semimetal’ at low energies, by gapping out a large fraction of complementary Fermi level density of states while leaving the vHS largely unspoiled. We show that this holds for recently discovered variant ScV_6Sn_6 [24], in contrast to AV_3Sb_5 in which the CDW develops within the same orbitals as a possible excitonic state [25]. Developing a minimal model for this material, we find s -wave and d -wave excitonic states as a function of interaction parameters, the latter of which offers an explanation of the nematic state recently seen in STM [26]. The excitonic scenario we develop for ScV_6Sn_6 provides a theoretical reconciliation of several experimental facts, and suggests novel signatures in optical spectroscopy.

Ab initio theory and minimal model. ScV_6Sn_6 is a paramagnetic metal belonging to a large family of related 166 compounds [27–29] of the form AM_6X_6 (e.g. $A=\text{Tb, Ho, Sc}$; $M=\text{V, Cr, Fe}$; $X=\text{Si, Ge, Sn}$) and consists of a kagome bilayer structure comprising a triangular lattice of scandium interposed with a honeycomb lattice of tin, two triangular lattices and a honeycomb lattice of vanadium atoms (Fig. 1). The high temperature phase belongs to the space group $P6/mmm$ (SG 191) [24, 30, 31], and is reduced to $R\bar{3}m$ (SG 166) [66] by a first-order transition at 92 K to a $(\frac{1}{3}, \frac{1}{3}, \frac{1}{3})$ CDW phase. Above T_{CDW} , fluctuations at $(\frac{1}{3}, \frac{1}{3}, \frac{1}{2})$ are observed but do not order [34–36], suggesting a competing CDW order also seen in first principles calculations [37–39].

The CDW is primarily concentrated on the Sn and Sc layers, and is largely absent on the vanadium kagome layers, as is known from STM [31] and the lack of a gap observed on the vanadium bands [40–45]. This can be understood physically – the CDW originates from the softening of an out-of-plane phonon mode corresponding to oscillations of the Sn and Sc atoms [46], which behave roughly as a set of weakly coupled one-dimensional chains. Substitution of Sc with larger rare earth ions inhibit the Sn-Sn oscillations, explaining the doping suppression of the CDW [47]. In contrast to the Sb p -orbitals in AV_3Sb_5 , the Sn p_z orbitals contribute much more weakly to the Fermi surface – via trigonal rather than hexagonal Sn – hybridizing with the V atoms to produce k_z dispersion [36] rather than contributing significantly to the in-plane dispersion, which is primarily derived from the V d -orbitals.

The CDW is more rapidly suppressed with applied pressure or doping compared to AV_3Sb_5 , though superconductivity has not been seen in this material, at any pressure or doping explored to date [47, 48]. This suggests a further comparison with AV_3Sb_5 : one viewpoint holds that superconductivity is driven by the Sb Γ -pocket; an analogous Sn band is absent in the 166 family.

The materials are significantly more three dimensional than the AV_3Sb_5 series, due to the hybridization with the out-of-plane Sn orbitals – as reflected by the three-

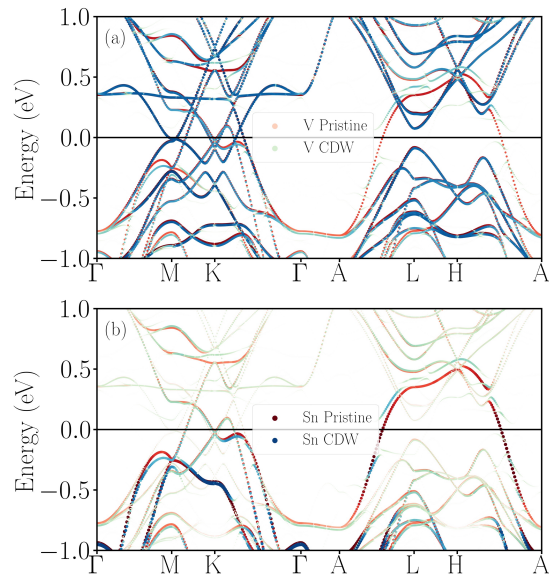


FIG. 2: **Ab-initio bandstructure in the pristine and CDW phase of ScV_6Sn_6 .** DFT bands above (red) and below (green) the CDW transition, with V and Sn orbital weights. For better visualization, the Sn weights are scaled by a factor four times greater than the V weights. The band crossing the Fermi level in the $k_z = 1/2$ plane derives from the hybridization between p_z orbitals of Sn atoms and V atoms; the associated spectral weight is gapped out by the CDW, producing a more two-dimensional electronic structure.

dimensional character of the dispersion shown in Fig. 2. This is also borne out in the lower transport anisotropy $\rho_c/\rho_{ab} \approx 5$ [50, 51] and relative difficulty of cleaving samples [42]. Yet, the spectral weight associated to the p -orbitals of the Sn atoms is gapped out upon the onset of the CDW, resulting in a significantly more two-dimensional dispersion, as well as pushing the two vHS closer to the Fermi level, Fig. 2, also reflected in the Fermi surface plots shown in the Supplementary Material (SM). As the CDW primarily affects the Sn and Sc atoms, the V-based kagome bandstructure remains intact.

Hence, we can construct a minimal model of ScV_6Sn_6 inside the CDW phase consisting of two effective d orbitals per site on a kagome bilayer, representing the twelve bands predominantly composed of the vanadium $d_{x^2-y^2}/d_{xy}$ and d_{z^2} orbitals respectively, corresponding to the A_{2g} and A_{1g} representations of the site symmetry group respectively. Since the dispersion arising from vanadium orbitals varies minimally along the k_z direction inside the CDW phase, we work with a model that neglects the hoppings along the z direction. Moving from layer basis to the basis of mirror eigenstates ($|\text{top}\rangle \pm |\text{bottom}\rangle)/\sqrt{2}$, the bands decouple into four sets of kagome bands with distinct mirror eigenvalues; projecting onto the two which cross the Fermi level, we obtain

$$\mathcal{H} = - \sum_{i, \sigma \neq \sigma'} t_\alpha \psi_{i\alpha\sigma}^\dagger \psi_{j\alpha\sigma'} + \sum_i \varepsilon_\alpha \psi_{i\alpha\sigma}^\dagger \psi_{i\alpha\sigma} \quad (1)$$

where $\alpha = z, x$ indexes the two orbitals, σ sublattice,

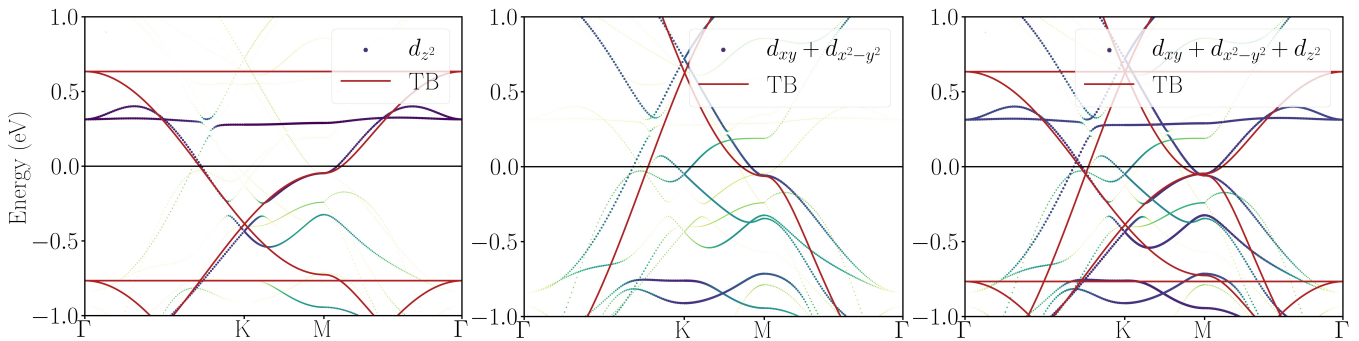


FIG. 3: **Minimal model compared with DFT.** Comparison between orbitally-projected DFT bands, in the pristine phase case, and the two-orbital tight-binding model, Eq. (1). Orbital weight varies from dark blue (large) to yellow (small).

$t_x = 0.69$ eV is the in-plane hopping between the d_{xy} -like orbitals, $t_z = -0.34$ eV is the in-plane hopping between the d_{z^2} orbitals, and additionally, the two sets of orbitals possess different onsite energies, $\varepsilon_z = -0.77$ eV and $\varepsilon_x = 1.35$ eV. Comparison between DFT and tight-binding in Fig. 3 indicates good agreement [67].

A key purpose of our minimal model is to accurately characterize the two vHS located close to the Fermi level, producing electron-like and hole-like Fermi surfaces with an approximate emergent particle-hole symmetry, consistent with prior ab-initio studies [46] and ARPES [44, 45] which observe two oppositely-dispersing vHS. The kagome tight-binding model exhibits a novel wavefunction structure near the vHS – referred to as the sublattice interference effect. Namely, the wavefunctions possess support either on one sublattice (pure, or p -type, sublattice support) or two (mixed, or m -type, sublattice support). We note importantly that the two vHS near the Fermi level are both p -type – as illustrated in Fig. 4. The plot of the charge density obtained from DFT shows that near a

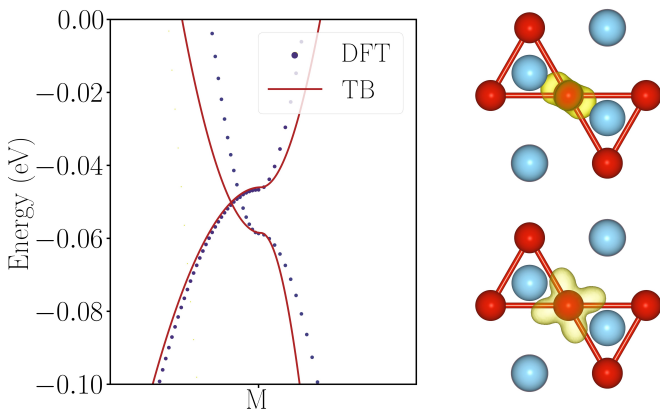


FIG. 4: **Pure type sublattice composition of the two vHS near the Fermi level.** (Left) Close up of the vHS arising from the two orbital model, compared with DFT. The upper vHS mainly has $V d_{z^2}$ character, while the lower vHS mainly has $V d_{xy} + d_{x^2-y^2}$ character. Right: Top-view of the partial charge density near M for the upper vHS with d_{z^2} character (top) and lower vHS with $d_{x^2-y^2}/d_{xy}$ character (bottom). In agreement with the p -type nature of the vHS, only one of three sites contributes.

given M -point, the wavefunction of both bands is concentrated entirely on one sublattice. An accurate reflection of the sublattice support plays an important role in our analysis of interaction effects.

Excitonic order. The emergence of excitons can be understood as a two-particle pairing problem: we first perform a particle-hole transformation, taking the valence electron with negative vHS concavity to a hole with positive concavity. The conduction electron and hole then have same dispersion but opposite charge. The bare Coulomb repulsion then becomes an effective attraction, driving the formation of bound states. The questions we address here are: (i) can these bound states condense, and (ii) in which spatial irrep do they condense.

On point (i): the two vHS cross each other, forming a ‘kagome semimetal’; if this band-crossing lies directly at the Fermi level, then for arbitrarily small dimensionless Coulomb interaction g , there exists a non-zero critical temperature at which excitons condense [68]. If the vHS cross away from Fermi level, as in ScV_6Sn_6 , then there is an energy cost $\delta\varepsilon$ to create particle-hole pairs, which then appear as gapped states with some lifetime. Upon including interactions, the exciton has a total energy $\delta\varepsilon - \varepsilon_b$, where ε_b is the binding energy. For $\varepsilon_b > \delta\varepsilon$, condensation occurs; this requires a minimum coupling strength g^* such that $\delta\varepsilon = \Lambda e^{-1/\sqrt{g^*}}$, where Λ is an energy cutoff [69]. For ScV_6Sn_6 , the relatively small $\delta\varepsilon \approx 20$ meV [44] suggests a tendency towards condensation.

To address point (ii), we present an analysis of excitonic order at mean field level in a minimal interacting model. The interactions which contribute to the mean-field equations are those which couple electrons and holes, which in our model correspond to the $d_{x^2-y^2}/d_{xy}$ and d_{z^2} orbitals. In the SM, we present a larger set of onsite and nearest-neighbour inter-orbital Hubbard interactions, but here we present a minimal case invoking an onsite inter-orbital U' , and nearest neighbour orbital exchange interaction V' ,

$$H_{\text{int}} = \sum_{i,\sigma\sigma',\alpha\neq\alpha'} U' \delta_{\sigma\sigma'} (\psi_{i\alpha\sigma}^\dagger \psi_{i\alpha\sigma}) (\psi_{i\alpha'\sigma}^\dagger \psi_{i\alpha'\sigma}) + V' (1 - \delta_{\sigma\sigma'}) (\psi_{i\alpha\sigma}^\dagger \psi_{i\alpha'\sigma}) (\psi_{i\alpha'\sigma}^\dagger \psi_{i\alpha\sigma}) \quad (2)$$

with α and σ the orbital and sublattice indices, and

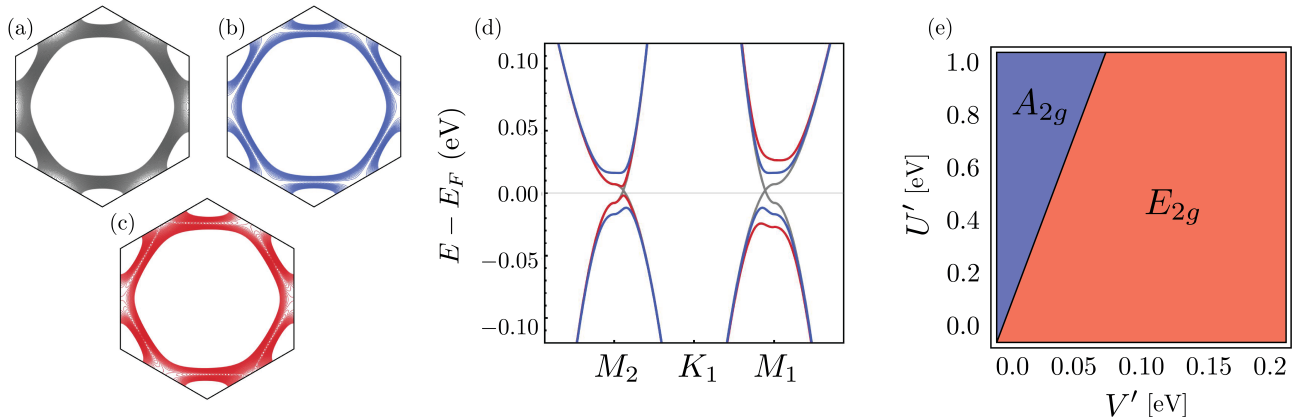


FIG. 5: **Mean-field excitonic states.** Contour plots of the minimal model (a) without excitonic order, and in the presence of (b) A_{1g} excitonic order, and (c) one component of E_{2g} excitonic order. Also shown (d) band structure cut with same colour coding. (e) Phase diagram as a function of onsite and nearest-neighbour inter-orbital Hubbard parameters.

$U', V' > 0$. We denote the creation operators for electron and hole-like fermions in band basis as $c_{\mathbf{k}}^{\dagger}$ and $d_{\mathbf{k}}^{\dagger}$, related to the sublattice σ basis via the unitary transformation $u_{\mathbf{k},+, \sigma} c_{\mathbf{k}}^{\dagger} = \psi_{\mathbf{k},+, \sigma}^{\dagger}$ and $u_{\mathbf{k},-, \sigma} d_{\mathbf{k}}^{\dagger} = \psi_{\mathbf{k},-, \sigma}^{\dagger}$. Defining the vertex form factors $F_{\mathbf{k}_1, \mathbf{k}_2; \sigma_1, \sigma_2}^{\mu\nu} = u_{\mathbf{k}_1, \mu, \sigma_1}^* u_{\mathbf{k}_2, \nu, \sigma_2}$, and performing the mean-field decomposition for $\Phi_{\mathbf{k}} = \langle c_{\mathbf{k}}^{\dagger} d_{\mathbf{k}} \rangle$ we arrive at the excitonic gap equation,

$$\Phi_{\mathbf{k}_1} = \sum_{\mathbf{k}_2, \sigma, \sigma'} [U' \delta_{\sigma, \sigma'} - 2V'(1 - \delta_{\sigma, \sigma'})] \times |F_{\mathbf{k}_1, \mathbf{k}_2; \sigma \sigma'}|^2 \Pi_{\mathbf{k}_2} \Phi_{\mathbf{k}_2} \quad (3)$$

with $\Pi_{\mathbf{k}}$ the particle-hole susceptibility (see the SM). We shift the vHS to lie exactly at the Fermi level and solve numerically for $\Phi_{\mathbf{k}}$ in the s - and d -wave like irreps, $\Gamma_{\Phi} = \{A_{1g}, E_{2g}\}$. Note that due to the Perron-Frobenius theorem, the lowest energy bound state of a purely attractive interaction potential will always be the A_{1g} state – a theorem well-noted in the context of superconducting instabilities [52]. Similarly, a purely attractive potential, such as that arising from U' , will always favor A_{1g} excitons. The orbital exchange term $-2V' < 0$ generates repulsion for excitons on different sublattices – and hence at different vHS, due to the p -type sublattice support – facilitating the appearance of E_{2g} order.

The symmetry representation Γ of the excitonic state is a product of the irreps of the c and d bands with the transformation of $\Phi_{\mathbf{k}}$ in momentum space, $\Gamma = \Gamma_{\Phi} \otimes \Gamma_c \otimes \Gamma_d$. Interestingly, since the c and d bands possess different symmetries, this results in the A_{1g} solution for Φ corresponding to an A_{2g} order parameter, transforming non-trivially under mirror when taking into account the symmetry properties of the orbitals [70].

We plot the resulting Fermi surface for both order parameters in Fig. 5a-c, alongside the associated bandstructure along a high-symmetry cut. For the A_{2g} solution, the two vHS are gapped out completely, while for a single E_{2g} solution the vHS remain gapless at one of the M points. We present the full momentum dependence of the eigenvectors in the SM. We find the excitonic state

is very sensitive to the orbital exchange interaction V' in our simplified model, developing in the E_{2g} channel for small $V'/U' \gtrsim 0.1$, as shown in Fig. 5e. In the SM, we present additional parameter space which illustrate that other inter-orbital Hubbard parameters can make the A_{2g} state more competitive.

The excitonic state breaks an approximate $U(1)$ symmetry associated to the difference in particle number of electrons and holes. Since this is not a microscopically conserved quantity, we expect small explicit symmetry breaking terms to pin the complex phase of this order parameter at low temperatures – either due to interorbital hopping terms, which are known to be parametrically weak [53], or ‘orbital umklapp’ interactions. Such effects break the emergent $U(1)$ to a residual \mathbb{Z}_2 , producing excitonic states that are either purely real or imaginary [71]. A purely imaginary A_{2g} state couples directly to magnetic field – this state has the symmetries of a ‘flux phase’, and unusually, breaks time-reversal symmetry despite being a single component order parameter.

The E_{2g} solutions to the gap equation are twofold degenerate, $\varphi_{1,2}$. The ground state may consist of a chiral combination of these two states $\varphi_1 + i\varphi_2$, or else a nematic real combination e.g. $\varphi_1 + \varphi_2$. Magnetotransport and μ SR see evidence of “soft orbital ferromagnetism” – weak signatures of time-reversal symmetry breaking which are enhanced in an applied field [54, 55]; the A_{2g} flux and chiral d -wave orders are both possible candidates for time-reversal symmetry breaking, which may be enhanced over the nematic combination by an applied field. While generically a mean-field computation of the Landau-Ginzburg free energy favours the chiral combination $\varphi_1 + i\varphi_2$, strained samples can produce nematic order [56]. We also note that there are cases in which variational methods find strong Coulomb repulsion results in a nodal rather than fully-gapped chiral state, despite the expectations of mean-field theory [57, 58].

Discussion. In this work we have developed a minimal model for ScV_6Sn_6 in the CDW phase, and proposed that the system hosts excitonic order, discussing some

candidate states based on a minimal model and offering an explanation of recent experiments. We find both a fully gapped phase which preserves time-reversal symmetry, and a nematic state which breaks rotational symmetry and selectively gaps the vHS – both states being possibly relevant to experiment. STM studies on kagome surface terminations observe nematic order around 70 K – clearly distinguished from the CDW, which is absent on the kagome surface [26]. Quasiparticle interference imaging observes a gap at the vHS at two of the three sets of M -points at this temperature; the appearance of a gap at the crossing between two oppositely-dispersing bands is a direct signature of an excitonic state. The excitonic state may also be related to the transport signatures of a second transition within the CDW phase [50], and weak spectral features seen near the vanadium vHS [59, 60].

We lastly discuss more direct experimental probes of excitonic physics. Above the temperature at which excitons condense, they appear as excitations of the system with an energy that gradually reduces upon approaching the critical temperature. Excitons with zero center of mass momentum are referred to as ‘bright’, and ‘dark’ otherwise; the translationally-invariant nature of our excitonic order parameter means the associated excitons are bright. Optical spectroscopy is a powerful tool to probe for such resonances; observing these excitations requires the exciton energy to be sufficiently large and to exceed the linewidth induced by various scattering processes.

Our related theoretical work in Ref. [25] predicted the appearance of such states in kagome metal CsV_3Sb_5 , where they are expected to appear as bright resonances inside the CDW gap, due to coexistence of excitons with CDW of the same orbital content. In the case of

ScV_6Sn_6 , excitons form in a parent bandstructure which is semimetallic, which makes observation of these resonances more challenging as they are expected to be broad due to coupling with the electronic continuum. Excitons in the former situation are similar to those in transition metal dichalcogenides [64], whereas those in the latter are analogous to those in candidate excitonic insulator Ta_2NiSe_5 , a zero-gap semiconductor [65].

In both the case of ScV_6Sn_6 and AV_3Sb_5 , the coexisting metallic bands which do not form excitons comprise different orbital content, suggesting that matrix element effects may suppress the exciton scattering rate and permit a feasible resolution; we leave a theoretical analysis of this possibility to future work, but suggest experimental investigation is the best approach to answer these questions.

Acknowledgements

JI thanks Riccardo Comin, Zurab Guguchia, Xiong Huang, Yu-Xiao Jiang, Chenhao Jin, Asish Kundu, William Meier, and Abhay Pasupathy for helpful discussions and comments. AC and RT acknowledge useful conversations with Matteo Dürnagel, Werner Hanke, Steve Kivelson, and Riccardo Sorbello. A.C. acknowledges support from PNRR MUR project PE0000023-NQSTI. A.C., D.D.S. and R.T. acknowledge the Gauss Centre for Supercomputing e.V. (<https://www.gauss-centre.eu>) for funding this project by providing computing time on the GCS Supercomputer SuperMUC-NG at Leibniz Supercomputing Centre (<https://www.lrz.de>).

-
- [1] R. L. Johnston and R. Hoffmann, “The kagome net - band theoretical and topological aspects”, *Polyhedron* **9**, 1901–1911 (1990).
 - [2] S.-L. Yu and J.-X. Li, “Chiral superconducting phase and chiral spin-density-wave phase in a Hubbard model on the kagome lattice”, *Phys. Rev. B* **85**, 144402 (2012).
 - [3] J. Wen et al., “Interaction-driven topological insulators on the kagome and the decorated honeycomb lattices”, *Phys. Rev. B* **82**, 075125 (2010).
 - [4] M. L. Kiesel, C. Platt and R. Thomale, “Unconventional Fermi Surface Instabilities in the Kagome Hubbard Model”, *Phys. Rev. Lett.* **110**, 126405 (2013).
 - [5] M. L. Kiesel and R. Thomale, “Sublattice interference in the kagome Hubbard model”, *Phys. Rev. B* **86**, 121105(R) (2012).
 - [6] T. Li et al., “Higher-order topological superconductivity from repulsive interactions in kagome and honeycomb systems”, *2D Mater.* **9** 015031 (2022).
 - [7] Y. Wang et al., “Quantum states and intertwining phases in kagome materials”, *Nat. Rev. Phys.* **5**, 635–658 (2023).
 - [8] J.-X. Yin, B. Lian and M. Z. Hasan, “Topological kagome magnets and superconductors”, *Nature* **612**, 647–657 (2022).
 - [9] B. R. Ortiz et al., “ CsV_3Sb_5 : A \mathbb{Z}_2 Topological Kagome Metal with a Superconducting Ground State”, *Phys. Rev. Lett.* **125**, 247002 (2020).
 - [10] S. D. Wilson and B. R. Ortiz, “ AV_3Sb_5 kagome superconductors”, *Nat. Rev. Mater.* **9**, 420–432 (2024).
 - [11] K. Jiang et al., “Kagome superconductors AV_3Sb_5 ($A = \text{K, Rb, Cs}$)”, *Natl. Sci. Rev.* **10**, nwac199 (2023).
 - [12] H. Yang et al., Superconductivity and orbital-selective nematic order in a new titanium-based kagome metal CsTi_3Bi_5 , [arXiv:2211.12264](https://arxiv.org/abs/2211.12264).
 - [13] B. Liu et al., “Tunable van Hove singularity without structural instability in kagome metal CsTi_3Bi_5 ”, *Phys. Rev. Lett.* **131**, 026701 (2023).
 - [14] H. Li et al., “Rotation symmetry breaking in the normal state of a kagome superconductor KV_3Sb_5 ”, *Nat. Phys.* **18**, 265–270 (2022).
 - [15] L. Nie et al., “Charge-density-wave-driven electronic nematicity in a kagome superconductor”, *Nature* **604**, 59 (2022).
 - [16] H. Li et al., “Electronic nematicity without charge density waves in titanium-based kagome metal”, *Nat. Phys.* **19**, 1591–1598 (2023).
 - [17] Z. Jiang et al., “Flat bands, non-trivial band topology

- and rotation symmetry breaking in layered kagome-lattice RbTi₃Bi₅”, *Nat. Commun.* **14**, 4892 (2023).
- [18] Y. Xu et al., “Three-state nematicity and magneto-optical Kerr effect in the charge density waves in kagome superconductors”, *Nat. Phys.* **18**, 1470–1475 (2022).
- [19] Y.-X. Jiang et al., “Unconventional chiral charge order in kagome superconductor KV₃Sb₅”, *Nat. Mater.* **20**, 1353–1357 (2021).
- [20] H. Chen et al., “Roton pair density wave and unconventional strong-coupling superconductivity in a topological kagome metal”, *Phys. Rev. X* **11**, 031026 (2021).
- [21] L. V. Keldysh and Y. V. Kopaev, “Possible instability of the semimetallic state toward Coulomb interaction”, *Sov. Phys. Solid State* **6**, 2219 (1965).
- [22] D. Jérôme, T. M. Rice, and W. Kohn, “Excitonic insulator”, *Phys. Rev.* **158**, 462 (1967).
- [23] B. Halperin and T. Rice, “The excitonic state at the semiconductor-semimetal transition”, *J. Phys. C: Solid State Phys.* **21**, 115 (1968).
- [24] H. W. S. Arachchige et al., “Charge Density Wave in Kagome Lattice Intermetallic ScV₆Sn₆”, *Phys. Rev. Lett.* **129**, 216402 (2022).
- [25] H. D. Scammell, J. Ingham, T. Li, and O. P. Sushkov, “Chiral excitonic order from twofold van Hove singularities in kagome metals”, *Nat. Commun.* **14**, 605 (2023).
- [26] Y.-X. Jiang et al., “Van-Hove annihilation and nematic instability on a Kagome lattice”, *Nat. Mater.* **23**, 1214–1221 (2024).
- [27] Y. Jiang et al., “Kagome Materials II: SG 191: FeGe as a LEGO Building Block for the Entire 1:6:6 series: hidden d-orbital decoupling of flat band sectors, effective models and interaction Hamiltonians”, [arXiv:2311.09290](https://arxiv.org/abs/2311.09290) (2023).
- [28] H. Hu et al., “Kagome Materials I: SG 191, ScV₆Sn₆. Flat Phonon Soft Modes and Unconventional CDW Formation: Microscopic and Effective Theory”, [arXiv:2305.15469](https://arxiv.org/abs/2305.15469).
- [29] D. Di Sante et al., “Flat band separation and robust spin Berry curvature in bilayer kagome metals”, *Nat. Phys.* **19**, 1135–1142 (2023).
- [30] Y. Gu et al., “Phonon mixing in the charge density wave state of ScV₆Sn₆”, *npj Quantum Mater.* **8**, 58 (2023).
- [31] Y. Hu et al., “Phonon promoted charge density wave in topological kagome metal ScV₆Sn₆”, *Nat. Commun.* **15**, 1658 (2024).
- [32] Y. Hinuma et al., “Band structure diagram paths based on crystallography”, *Computational Materials Science* **128**, 140–184 (2017).
- [33] A. Togo, K. Shinohara, and I. Tanaka, “Spglib: a software library for crystal symmetry search”, [arXiv 1808.01590](https://arxiv.org/abs/1808.01590) (2024).
- [34] G. Pokharel et al., “Frustrated charge order and cooperative distortions in ScV₆Sn₆”, *Phys. Rev. Materials* **7**, 104201 (2023).
- [35] S. Cao et al., “Competing charge-density wave instabilities in the kagome metal ScV₆Sn₆”, *Nat. Commun.* **14**, 7671 (2023).
- [36] A. Korshunov et al., “Softening of a flat phonon mode in the kagome ScV₆Sn₆”, *Nat. Commun.* **14**, 6646 (2023).
- [37] H. Tan and B. Yan, “Abundant Lattice Instability in Kagome Metal ScV₆Sn₆”, *Phys. Rev. Lett.* **130**, 266402 (2023).
- [38] S. Liu et al., “Driving Mechanism and Dynamic Fluctuations of Charge Density Waves in the Kagome Metal ScV₆Sn₆” *Phys. Rev. B* **109**, L121103 (2024).
- [39] A. Subedi, “Order-by-disorder charge density wave condensation at $q = (\frac{1}{3}, \frac{1}{3}, \frac{1}{3})$ in kagome metal ScV₆Sn₆”, *Phys. Rev. Materials* **8**, 014006 (2024).
- [40] T. Hu et al., “Optical spectroscopy and band structure calculations of the structural phase transition in the vanadium-based kagome metal ScV₆Sn₆”, *Phys. Rev. B* **107**, 165119 (2023).
- [41] D. W. Kim et al., “Infrared probe of the charge density wave gap in ScV₆Sn₆”, *Phys. Rev. B* **108**, 205118 (2023).
- [42] S.-H. Kang et al., “Emergence of a new band and the Lifshitz transition in kagome metal ScV₆Sn₆ with charge density wave” [arXiv:2302.14041](https://arxiv.org/abs/2302.14041).
- [43] Z.-J. Cheng et al., “Untangling charge-order dependent bulk states from surface effects in a topological kagome metal ScV₆Sn₆”, *Phys. Rev. B* **109**, 075150 (2024).
- [44] S. Lee et al., “Nature of charge density wave in kagome metal ScV₆Sn₆”, *npj Quantum Mater.* **9**, 15 (2024).
- [45] A. K. Kundu et al., “Low-energy electronic structure in the unconventional charge-ordered state of ScV₆Sn₆”, *Nat. Commun.* **15**, 5008 (2024).
- [46] M. Tuniz et al., “Dynamics and resilience of the unconventional charge density wave in ScV₆Sn₆ bilayer kagome metal”, *Commun. Mater.* **4**, 103 (2023).
- [47] W. R. Meier et al., “Tiny Sc allows the chains to rattle: Impact of Lu and Y doping on the charge density wave in ScV₆Sn₆”, *J. Am. Chem. Soc.* **145**, 38, 20943 (2023).
- [48] C. Yi et al., “Tuning charge density wave of kagome metal ScV₆Sn₆”, *New J. Phys.* **26** 052001 (2024).
- [49] X. Zhang et al., “Destabilization of the Charge Density Wave and the Absence of Superconductivity in ScV₆Sn₆ under High Pressures up to 11 GPa”, *Materials* **15**, 7372 (2022).
- [50] S. Mozaffari et al., “Universal sublinear resistivity in vanadium kagome materials hosting charge density waves”, *Phys. Rev. B* **110**, 035135 (2024).
- [51] J. M. DeStefano et al., “Pseudogap behavior in charge density wave kagome material ScV₆Sn₆ revealed by magnetotransport measurements”, *npj Quantum Mater.* **8**, 65 (2023).
- [52] M. S. Scheurer, “Mechanism, time-reversal symmetry, and topology of superconductivity in noncentrosymmetric systems”, *Phys. Rev. B* **93**, 174509 (2016).
- [53] X. Wu et al., “Nature of unconventional pairing in the kagome superconductors AV₃Sb₅”, *Phys. Rev. Lett.* **127**, 177001 (2021).
- [54] Z. Guguchia et al., “Hidden magnetism uncovered in charge ordered bilayer kagome material ScV₆Sn₆”, *Nat. Commun.* **14**, 7796 (2023).
- [55] C. Yi et al., “Quantum oscillations revealing topological band in kagome metal ScV₆Sn₆”, *Phys. Rev. B* **109**, 035124 (2024).
- [56] M. Sigrist and K. Ueda, “Phenomenological theory of unconventional superconductivity”, *Rev. Mod. Phys.* **63**, 239 (1991).
- [57] T. Grover, N. Trivedi, T. Senthil and P. A. Lee, “Weak Mott insulators on the triangular lattice: Possibility of a gapless nematic quantum spin liquid”, *Phys. Rev. B* **81**, 245121 (2010).
- [58] D. Guerci, D. Kaplan, J. Ingham, J. H. Pixley, A. J. Millis, “Topological superconductivity from repulsive interactions in twisted bilayer WSe₂”, [arXiv:2408.16075](https://arxiv.org/abs/2408.16075).
- [59] S. Chen et al., “Nanoscale visualization and spectral fingerprints of the charge order in ScV₆Sn₆ distinct from other kagome metals”, *npj Quantum Mater.* **9**, 14 (2024).
- [60] Y.-C. Yang et al., “Unveiling the charge density wave

- mechanism in vanadium-based Bi-layered kagome metals”, *npg Asia Mater.* **16**, 46 (2024).
- [61] K. Shrestha et al., “Electronic properties of kagome metal ScV_6Sn_6 using high field torque magnetometry”, *Phys. Rev. B* **108**, 245119.
- [62] R. Guehne et al., “Orbital selective commensurate modulations of the local density of states in ScV_6Sn_6 probed by nuclear spins”, *Nat. Commun.* **15**, 8213 (2024).
- [63] T. Yu et al., “Magnetism and weak electronic correlations in the kagome metal”, *Phys. Rev. B* **109**, 195145 (2024).
- [64] G. Wang et al., “Colloquium: Excitons in atomically thin transition metal dichalcogenides”, *Rev. Mod. Phys.* **90**, 021001 (2018).
- [65] Y. F. Lu et al., “Zero-gap semiconductor to excitonic insulator transition in Ta_2NiSe_5 ”, *Nat. Commun.* **8**, 14408 (2017).
- [66] The CDW structure originally reported in Ref. [24] is weakly inversion symmetry breaking, corresponding to R32 (SG 155, c.f. [32, 33]).
- [67] Ref. [27] has also discussed tight-binding minimal models for 166 and the related 1:1 compounds. The models considered there apply to the pristine phase including the Sn p orbitals, whereas our present model neglects the role of the p orbitals, which we justify with resort to the effect of the CDW on the Sn spectral weight (Fig. 2).
- [68] The origin of weak-coupling instability towards exciton condensation can be understood as ‘zero wavevector nesting’: as is well known, when the Fermi surface possesses the nesting property $\varepsilon(\mathbf{k}) = -\varepsilon(\mathbf{k} + \mathbf{Q})$ for some wavevector \mathbf{Q} , the Fermi surface becomes unstable towards the formation of a spin or charge density wave $\langle c_{\mathbf{k}+\mathbf{Q}}^\dagger c_{\mathbf{k}} \rangle \neq 0$. In the presence of two Fermi surfaces c and d with $\varepsilon_c(\mathbf{k}) = -\varepsilon_d(\mathbf{k})$, one finds the nesting condition satisfied with $\mathbf{Q} = 0$, indicating an instability towards a state which hybridizes the two Fermi surfaces $\langle c_{\mathbf{k}}^\dagger d_{\mathbf{k}} \rangle \neq 0$.
- [69] The $e^{-1/\sqrt{g}}$ dependence, rather than the $e^{-1/g}$ typical of BCS-like instabilities, appears due to the enhanced density of states near a vHS.
- [70] The symmetry behaviour of the E_{2g} state is unchanged upon taking into account the band representations.
- [71] This is akin to the appearance of purely real and imaginary CDW states – rCDW and iCDW – in patch models, which arises due to conventional umklapp interactions between the different vHS breaking an emergent “patch conservation” symmetry, which would otherwise produce complex CDW orders with an arbitrary $U(1)$ phase.
-

Supplementary Material

S1. BANDSTRUCTURE DETAILS

Density functional theory calculations were performed with the Vienna ab initio Simulation Package (VASP) [S1, S2], using the projector augmented wave (PAW) method [S3]. Exchange and correlation effects have been included at the generalized gradient approximation (GGA) level [S4, S5, S7] within the Perdew-Burke-Ernzerhof (PBE) approach [S6]. The plane-wave cutoff used for the truncation of the basis set is 500 eV, both for the pristine and the CDW unit cells. In both cases the relaxation of the electronic and ionic degrees of freedom was considered converged when the output difference between two steps was equal or smaller than 1×10^{-6} eV and 1×10^{-6} eV/Å, respectively. The number of \mathbf{k} -points used for the pristine unit cell is $15 \times 15 \times 9$, while the CDW supercell it is $9 \times 9 \times 3$. Partial occupancies have been determined via Gaussian smearing with a width of 0.01 eV. Spin-orbit coupling has not been considered in this work. DFT band structures have been visualized using the VASPKIT postprocessing tool [S10], while VESTA [S11] has been used to visualize the crystal structures and the charge densities.

To complement our plots of the bandstructure in the main text, we present plots of the Fermi surface in Fig. 3, which make more explicit the increased two-dimensionality inside the CDW phase.

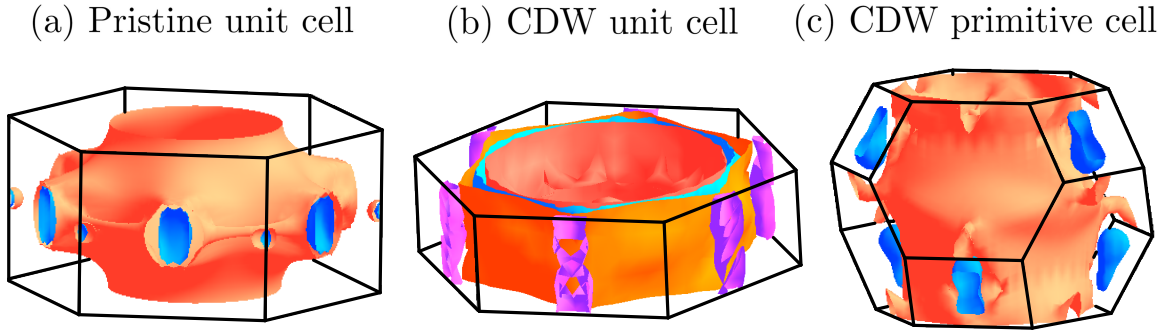


FIG. S1: **Fermi surfaces for ScV_6Sn_6 .** Fermi surface in the (a) pristine phase above T_{CDW} , and beneath T_{CDW} in the (b) unit cell, and (c) primitive cell.

S2. INTER-ORBITAL HUBBARD MODEL

In this section we discuss the mean-field analysis for excitonic order from short-ranged interactions. The interactions which generate excitonic order are those which couple the opposite concavity vHS, which are purely composed of the d_{z^2} and $d_{xy}/d_{x^2-y^2}$ orbitals respectively. The interactions which drive excitonic order are therefore strictly those which couple the two distinct orbital types, which we index by α as in the main text. We write down an extended Hubbard model featuring only couplings between different orbitals, and between both electrons onsite and on neighbouring sites i.e. adjacent sublattices indexed by σ . We will use slightly different notation to the main text to better compare with prior work [S12]; the U' and V' of the main text correspond to U_{h_4} and U_{l_2} below. The result is an interacting Hamiltonian,

$$\begin{aligned}
 H_{\text{int}} = & \sum_{i, (\sigma, \sigma'), \alpha \neq \alpha'} \left[U_{h_1} (\psi_{i, \alpha, \sigma}^\dagger \psi_{i, \alpha, \sigma'}) (\psi_{i, \alpha', \sigma'}^\dagger \psi_{i, \alpha', \sigma}) + U_{h_4} \delta_{\sigma, \sigma'} (\psi_{i, \alpha, \sigma}^\dagger \psi_{i, \alpha, \sigma}) (\psi_{i, \alpha', \sigma'}^\dagger \psi_{i, \alpha', \sigma'}) \right. \\
 & + U_{j_1} (\psi_{i, \alpha, \sigma}^\dagger \psi_{i, \alpha', \sigma'}) (\psi_{i, \alpha, \sigma'}^\dagger \psi_{i, \alpha', \sigma}) + U_{j_2} (\psi_{i, \alpha, \sigma}^\dagger \psi_{i, \alpha', \sigma}) (\psi_{i, \alpha, \sigma'}^\dagger \psi_{i, \alpha', \sigma'}) + U_{j_4} \delta_{\sigma, \sigma'} (\psi_{i, \alpha, \sigma}^\dagger \psi_{i, \alpha, \sigma}) (\psi_{i, \alpha', \sigma'}^\dagger \psi_{i, \alpha', \sigma'}) \\
 & \left. + U_{l_2} (\psi_{i, \alpha, \sigma}^\dagger \psi_{i, \alpha', \sigma'}) (\psi_{i, \alpha', \sigma'}^\dagger \psi_{i, \alpha, \sigma}) + U_{l_4} \delta_{\sigma, \sigma'} (\psi_{i, \alpha, \sigma}^\dagger \psi_{i, \alpha, \sigma}) (\psi_{i, \alpha', \sigma'}^\dagger \psi_{i, \alpha', \sigma'}) \right] \quad (\text{S1})
 \end{aligned}$$

Denoting the creation operators for electron and hole-like fermions in band basis as $c_{\mathbf{k}}^\dagger$ and $d_{\mathbf{k}}^\dagger$, the transformation to band basis is effected via the unitary transformation $u_{\mathbf{k}, +, \sigma} c_{\mathbf{k}}^\dagger = \psi_{\mathbf{k}, +, \sigma}^\dagger$ and $u_{\mathbf{k}, -, \sigma} d_{\mathbf{k}}^\dagger = \psi_{\mathbf{k}, -, \sigma}^\dagger$, as described in the main text. Fig. S2 represents the mean field equation for the excitonic order parameter $\Phi_{\mathbf{k}+}^C = \langle c_{\mathbf{k}}^\dagger d_{\mathbf{k}} \rangle$, with $\Phi_{\alpha+}^C = (\Phi_{\alpha-}^C)^\dagger$. The corresponding vertices appearing in Fig. S2 acquire form factors from the transformation to band

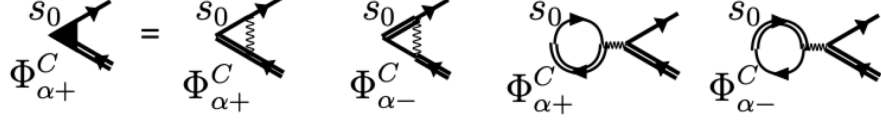


FIG. S2: **Diagrammatic contributions to the excitonic pairing vertex.** Diagrammatic representation of the mean-field equations for spin-singlet excitonic order, with $\Phi_{\alpha+}^C = \langle c_{\alpha}^{\dagger} d_{\alpha} \rangle$ and $\Phi_{\alpha+}^C = (\Phi_{\alpha-}^C)^{\dagger}$.

basis, which we denote as $F_{\mathbf{k}_1, \mathbf{k}_2; \sigma_1, \sigma_2}^{\mu\nu} = u_{\mathbf{k}_1, \mu, \sigma_1}^* u_{\mathbf{k}_2, \nu, \sigma_2}$, and using that $F_{\mathbf{k}_1, \mathbf{k}_2; \sigma_1, \sigma_2}^{++} = F_{\mathbf{k}_1, \mathbf{k}_2; \sigma_1, \sigma_2}^{--} \equiv F_{\mathbf{k}_1, \mathbf{k}_2; \sigma_1, \sigma_2}$ we will make use of $F_{\mathbf{k}_1, \mathbf{k}_1; \sigma_1, \sigma_1} F_{\mathbf{k}_2, \mathbf{k}_2; \sigma_2, \sigma_2} = |F_{\mathbf{k}_1, \mathbf{k}_2; \sigma_1, \sigma_2}|^2$. We may introduce shorthand notation for each vertex,

$$V_{\mathbf{k}_1, \mathbf{k}_2; \sigma_1, \sigma_2}^{++} = [U_{h_4} \delta_{\sigma_1, \sigma_2} + U_{h_1} (1 - \delta_{\sigma_1, \sigma_2})] |F_{\mathbf{k}_1, \mathbf{k}_2; \sigma_1, \sigma_2}|^2 \quad (S2)$$

$$B_{\mathbf{k}_1, \mathbf{k}_2; \sigma_1, \sigma_2}^{++} = [U_{l_4} \delta_{\sigma_1, \sigma_2} + U_{l_2} (1 - \delta_{\sigma_1, \sigma_2})] |F_{\mathbf{k}_1, \mathbf{k}_2; \sigma_1, \sigma_2}|^2 \quad (S3)$$

$$V_{\mathbf{k}_1, \mathbf{k}_2; \sigma_1, \sigma_2}^{+-} = [U_{j_4} \delta_{\sigma_1, \sigma_2} + U_{j_1} (1 - \delta_{\sigma_1, \sigma_2})] |F_{\mathbf{k}_1, \mathbf{k}_2; \sigma_1, \sigma_2}|^2 \quad (S4)$$

$$B_{\mathbf{k}_1, \mathbf{k}_2; \sigma_1, \sigma_2}^{+-} = [U_{j_4} \delta_{\sigma_1, \sigma_2} + U_{j_2} (1 - \delta_{\sigma_1, \sigma_2})] |F_{\mathbf{k}_1, \mathbf{k}_2; \sigma_1, \sigma_2}|^2 \quad (S5)$$

with $V^{\gamma_1, \gamma_2} = V^{\gamma_2, \gamma_1}$ and $B^{\gamma_1, \gamma_2} = B^{\gamma_2, \gamma_1}$ for $\gamma = \pm$. We distinguish the vertex contributions V , from the bubble diagrams B , and define the spinless particle-hole susceptibility $\Pi_{\mathbf{k}}$. Taken together, the self-consistent vertex equation can be cast as a simple eigenvalue problem,

$$\begin{pmatrix} \Phi_{\mathbf{k}_1}^+ \\ \Phi_{\mathbf{k}_1}^- \end{pmatrix} = \sum_{\mathbf{k}_2, \sigma_1, \sigma_2} \begin{pmatrix} V_{\mathbf{k}_1, \mathbf{k}_2; \sigma_1, \sigma_2}^{++} - 2B_{\mathbf{k}_1, \mathbf{k}_2; \sigma_1, \sigma_2}^{++} & V_{\mathbf{k}_1, \mathbf{k}_2; \sigma_1, \sigma_2}^{+-} - 2B_{\mathbf{k}_1, \mathbf{k}_2; \sigma_1, \sigma_2}^{+-} \\ V_{\mathbf{k}_1, \mathbf{k}_2; \sigma_1, \sigma_2}^{-+} - 2B_{\mathbf{k}_1, \mathbf{k}_2; \sigma_1, \sigma_2}^{-+} & V_{\mathbf{k}_1, \mathbf{k}_2; \sigma_1, \sigma_2}^{--} - 2B_{\mathbf{k}_1, \mathbf{k}_2; \sigma_1, \sigma_2}^{--} \end{pmatrix} \Pi_{\mathbf{k}_2} \begin{pmatrix} \Phi_{\mathbf{k}_2}^+ \\ \Phi_{\mathbf{k}_2}^- \end{pmatrix}. \quad (S6)$$

It remains to diagonalize $\bar{\Phi} = \hat{M}\bar{\Phi}$; we can further simplify the matrix to bring it to a form more familiar in patch treatments of vHS [S12–S19],

$$(\hat{M})_{\mathbf{k}_1, \mathbf{k}_2; \sigma_1, \sigma_2} = \begin{pmatrix} (U_{h_4} - 2U_{j_4})\delta_{\sigma_1, \sigma_2} + (U_{h_1} - 2U_{l_2})(1 - \delta_{\sigma_1, \sigma_2}) & -U_{j_4}\delta_{\sigma_1, \sigma_2} + (U_{j_1} - 2U_{j_2})(1 - \delta_{\sigma_1, \sigma_2}) \\ -U_{j_4}\delta_{\sigma_1, \sigma_2} + (U_{j_1} - 2U_{j_2})(1 - \delta_{\sigma_1, \sigma_2}) & (U_{h_4} - 2U_{j_4})\delta_{\sigma_1, \sigma_2} + (U_{h_1} - 2U_{l_2})(1 - \delta_{\sigma_1, \sigma_2}) \end{pmatrix} |F_{\mathbf{k}_1, \mathbf{k}_2; \sigma_1, \sigma_2}|^2 \Pi_{\mathbf{k}_2}. \quad (S7)$$

We explore the mean-field phase diagram by numerical diagonalization for various regions of parameter space. The key coupling which drives E_{2g} excitonic order are the orbital exchange interactions, as explained in the main text; retaining only U_{h_4} and U_{l_2} produces the phase diagram shown in Fig. 5 of the main text, in which small values of U_{l_2} already result in E_{2g} order. As illustrated by Fig. S3, various combinations of the other Hubbard parameters can promote the fully gapped A_{2g} state. We leave ab initio estimates of these interaction parameters to future work.

In addition to the effects of strain, as well as the orbital exchange couplings which we have already discussed, perturbative renormalization group analyses have shown that fluctuation effects beyond mean field theory may also favour E_{2g} order [S12], but such effects lie outside the scope of our present work.

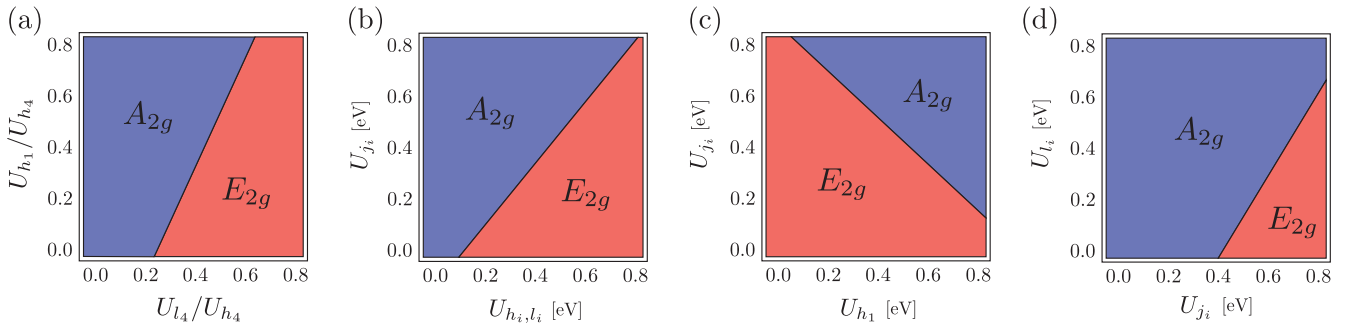


FIG. S3: **Phase diagram as a function of Hubbard parameters.** Plot of the state with largest eigenvalue of the gap equation as a function of the Hubbard parameters; all units of energy are in eV. In the notation of the main text, $U_{l_2} = V'$ and $U_{h_4} = U'$ (a) U_{h_1} versus U_{l_4} at fixed $U_{h_4} = 1$, with $U_{l_2} = U_{l_4}$ and $U_{j_1} = U_{j_2} = U_{j_4} = 0$. (b) Setting $U_{h_4} = 1$, and setting all $U_{l_i} = U_{h_1}$ versus U_{j_i} . (c) Taking values $U_{l_2} = U_{l_4} = 0.5$, $U_{h_4} = 1$, and comparing U_{j_i} against U_{h_1} . (d) Taking $U_{h_4} = 1$, $U_{h_1} = 0.75$, setting all U_{j_i} equal and U_{l_i} equal and plotting U_{l_i} against U_{j_i} .

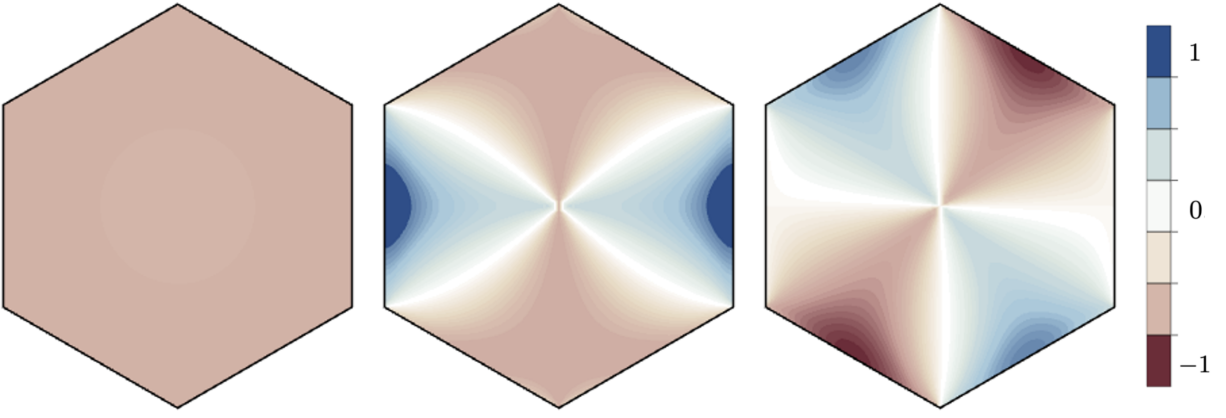


FIG. S4: **Momentum space structure of the gap equation solutions.** The eigenstates of Eq. (S6) for the three states with non-zero eigenvalue, for the case of $U_{h_4} \neq 0$ and all other interactions zero (presented in arbitrary units). The corresponding (normalized) eigenvalues are $\{1, 0.44, 0.44\}$ and zero for all other states, but the momentum space structure of the eigenvectors themselves is essentially the same for different choices of parameters. The eigenstates are seen to transform as $\Gamma_\Phi = \{A_{1g}, E_{2g}^{(1)}, E_{2g}^{(2)}\}$, while the full order parameter transforms as $\Gamma = \Gamma_\Phi \otimes A_{2g} = \{A_{2g}, E_{2g}^{(1)}, E_{2g}^{(2)}\}$.

The E_{2g} can be understood in momentum space as corresponding to sign changes as one traverses through the M points. Due to the p -type nature of each vHS, the E_{2g} can therefore be understood as in real space as sign changes occurring between sublattices. To illustrate the momentum space structure of the solutions, we plot the eigenvectors of the mean-field equations throughout the full Brillouin zone in Fig. S4 for $U_{h_4} = 1$ and all other couplings zero. Note that the largest eigenvalue (corresponding to the lowest energy bound state) in this case is the A_{1g} solution, but the E_{2g} state is nonetheless present as a solution due to the momentum dependence of the form factors.

The fact that a subleading E_{2g} order can arise even for the simple onsite U' interaction derives from the effects of the wavefunction form factors, which can and do add spatially varying prefactors to otherwise spatially structureless couplings [S20–S22]. We illustrate this point using analytical arguments. Consider exciton pairing in a patch about a given M point, say M_1 at which the wavefunctions are localized at A-sites. Using the approximate particle-hole symmetry, then

$$\begin{aligned} \Phi_{\mathbf{k}_1}^{M_1} &= U' \sum_{\mathbf{k}_2 \in \mathcal{P}(M_1)} \mathcal{U}_{\mathbf{k}_1,+,A}^* \mathcal{U}_{\mathbf{k}_2,+,A} \mathcal{U}_{\mathbf{k}_2,+,A}^* \mathcal{U}_{\mathbf{k}_1,+,A} \Phi_{\mathbf{k}_2}^{M_1} \\ &= U' \sum_{\mathbf{k}_2 \in \mathcal{P}(M_1)} |\mathcal{U}_{\mathbf{k}_1,+,A}|^2 |\mathcal{U}_{\mathbf{k}_2,+,A}|^2 \Phi_{\mathbf{k}_2}^{M_1} \end{aligned} \quad (\text{S8})$$

$$\Phi_{\mathbf{k}_1}^{M_1} \approx U' \sum_{\mathbf{k}_2 \in \mathcal{P}(M_1)} \Phi_{\mathbf{k}_2}^{M_1}. \quad (\text{S9})$$

We have used that $|\mathcal{U}_{\mathbf{k},+,A}|^2 \approx 1$ and $|\mathcal{U}_{\mathbf{k},+,B/C}|^2 \approx 0$ for $\mathbf{k} \approx M_1$. The approximate gap equation (S9) clearly has solution $\Phi_{\mathbf{k}_1}^{M_1} = \text{constant}$, and importantly, we see that it is even under all C_2 axes and mirrors. Accounting for all three patches, the eigenstates will decomposed into irreps of C_{3z} , giving just A, E . Taking into account the behaviour under the C_2 and mirrors, the A, E irreps of the patch theory become A_{1g}, E_{2g} of the continuous D_{6h} theory.

We emphasize that, following the discussion in the main text, the full symmetry of the order parameter is not only determined by the A/E form factor determined by solving the gap equation of our two-dimensional model, but the orbital content of the parent bands, which determine the symmetry behavior under out-of-plane symmetry operation M_z . The order parameter symmetry one expects in different kagome bilayer materials may therefore differ as a result of these considerations.

[S1] G. Kresse and D. Joubert, “From ultrasoft pseudopotentials to the projector augmented-wave method”, *Phys. Rev. B* **59**, 1758 (1999).

[S2] G. Kresse and J. Furthmüller, “Efficient iterative schemes for ab initio total-energy calculations using a plane-wave basis set”, *Phys. Rev. B* **54**, 11169 (1996).

- [S3] P. E. Blöchl, “Projector augmented-wave method”, *Phys. Rev. B* **50**, 17953 (1994).
- [S4] J. P. Perdew et al., “Atoms, molecules, solids, and surfaces: Applications of the generalized gradient approximation for exchange and correlation”, *Phys. Rev. B* **46**, 6671 (1992).
- [S5] A. D. Becke, “Density-functional exchange-energy approximation with correct asymptotic behavior”, *Phys. Rev. A* **38**, 3098 (1998).
- [S6] J. P. Perdew, K. Burke, and M. Ernzerhof, “Generalized Gradient Approximation Made Simple”, *Phys. Rev. Lett.* **77**, 3865 (1996).
- [S7] D. C. Langreth and M. J. Mehl, “Beyond the local-density approximation in calculations of ground-state electronic properties”, *Phys. Rev. B* **28**, 1809 (1983).
- [S8] G. H. Wannier, “The Structure of Electronic Excitation Levels in Insulating Crystals”, *Phys. Rev.* **52**, 191 (1937).
- [S9] G. H. Wannier, “Dynamics of Band Electrons in Electric and Magnetic Fields”, *Rev. Mod. Phys.* **34**, 645 (1962).
- [S10] V. Wang et al., “VASPKIT: A user-friendly interface facilitating high-throughput computing and analysis using VASP code”, *Comp. Phys. Commun.* **267**, 108033 (2021).
- [S11] K. Momma and F. Izumi, “*VESTA*: a three-dimensional visualization system for electronic and structural analysis”, *Journ. Appl. Cryst.* **41**, 653 (2008).
- [S12] H. D. Scammell, J. Ingham, T. Li, and O. P. Sushkov, “Chiral excitonic order from twofold van Hove singularities in kagome metals”, *Nat. Commun.* **14**, 605 (2023).
- [S13] S. Maiti and A. V. Chubukov, “Superconductivity from repulsive interaction”, *AIP Conference Proceedings* **1550**, 3 (2013).
- [S14] H. J. Schulz, “Superconductivity and Antiferromagnetism in the Two-Dimensional Hubbard Model: Scaling Theory”, *Europhys. Lett.* **4**, 609-615 (1987).
- [S15] N. Furukawa, T. M. Rice and M. Salmhofer, “Truncation of a Two-Dimensional Fermi Surface due to Quasiparticle Gap formation at the Saddle Points”, *Phys. Rev. Lett.* **81**, 3195-3198 (1998).
- [S16] L. Classen et al., “Competing orders at higher-order Van Hove points”, *Phys. Rev. B* **102**, 125141 (2020).
- [S17] R. Nandkishore, L. S. Levitov and A. V. Chubukov, “Chiral superconductivity from repulsive interactions in doped graphene”, *Nat. Phys.* **8**, 158-163 (2012).
- [S18] T. Park, M. Ye and L. Balents “Electronic instabilities of kagome metals: saddle points and Landau theory”, *Phys. Rev. B* **104**, 035142 (2021).
- [S19] P. K. Nab et al., “Pomeranchuk Instability Induced by an Emergent Higher-Order van Hove Singularity on the Distorted Kagome Surface of $\text{Co}_3\text{Sn}_2\text{S}_2$ ”, [arXiv:2410.01994](https://arxiv.org/abs/2410.01994).
- [S20] J. Ingham, T. Li, M. S. Scheurer, and H. D. Scammell, “Quadratic Dirac fermions and the competition of ordered states in twisted bilayer graphene”, [arXiv:2308.00748](https://arxiv.org/abs/2308.00748).
- [S21] H. D. Scammell, J. Ingham, M. Geier, and T. Li, “Intrinsic first and higher-order topological superconductivity in a doped topological insulator”, *Phys. Rev. B* **105**, 195149 (2022).
- [S22] T. Li, J. Ingham and H. D. Scammell “Artificial graphene: Unconventional superconductivity in a honeycomb superlattice”, *Phys. Rev. Research* **2**, 043155 (2020).